A New Approach for Calibrating High-voltage Capacitance and Dissipation Factor Bridges

Gregory A. Kyriazis

Instituto Nacional de Metrologia. Normalização e Qualidade Industrial
Duque de Caxias - RJ - Brazil
Email: gakyriazis@inmetro.gov.br

Abstract: A new approach for calibrating automated high-voltage current-comparator-based capacitance and dissipation factor bridges is presented. The approach is slightly different from another published previously. It leads to larger uncertainties, but is slightly easier to implement, since the digitizers need not be synchronized to the signal generators. It is possible to simulate capacitance ratios from 1:1 to 100:1 with relative standard uncertainties of less than $2.5 \cdot 10^{-5}$ and dissipation factors from 0 to 0.1 with standard uncertainties of less than $1 \cdot 10^{-5}$.

Keywords: calibration, sampling methods, capacitance, dissipation factor, ac bridge.

1. INTRODUCTION

Commercial automated high-voltage current-comparator-based capacitance and dissipation factor bridges [1][2] have been used extensively for calibrating high-voltage standard capacitors, shunt reactors and power transformers and for assessing the dielectric properties of power apparatus insulation with respect to safety, quality and service life.

Such bridges have been calibrated with gas-dielectric standard capacitors and dissipation factor standards [3] (see section 3 for constructive details of dissipation factor standards). Some shortcomings of this method are: (a) a high-voltage apparatus is required, (b) the number of test points is restricted to the number and values of the standards available, and (c) the dissipation factor uncertainty increases with the actual dissipation factor being measured, thus limiting the accuracy of loss measurements reported by bridge manufacturers.

A more flexible and accurate calibration procedure has been proposed in [4]. Neither high-voltage capacitors and dissipation factor standards nor a high-voltage source are required. The calibration of the bridge is carried out at low voltage. These bridges measure the ratio of their input currents. For the calibration, two sinusoidal currents are synthesized with the aid of a digital, programmable two-channel ac voltage source and two resistors. The complex ratio of these synthesized input currents is calculated from an ac voltage ratio determined by a sampling method, together with the impedance ratio of the resistors. The system uses a synchronous sampling technique, which requires the timing of the digital source to be obtained from the time base of the digitizer used to sample the voltage signals [5]. This allows the sampling interval to be selected according to the time base resolution of the digitizer so that each acquisition can cover one or more signal periods with high accuracy.

In [4], the voltage drops across the resistors are measured. It is not easy to measure such voltage drops with digital sampling voltmeters. A complex buffer arrangement is required to unload the digitizer inputs. Wagner balancing is also required to reduce the potential differences between the LOW terminals of the impedances and earth so that their influence on the impedance ratio can be negligible. In addition, the approach requires the digitizer to be synchronized to the signal generator.

A new approach for calibrating automated high-voltage current-comparator-based bridges is presented here. It leads to larger uncertainties, but is slightly easier to implement. For the calibration, two sinusoidal currents are synthesized with two synchronized signal generators and two resistors, and injected into the bridge inputs. Again, the capacitance ratio and dissipation factor simulated by these currents are calculated from an ac voltage ratio estimated from the digitized data, together with the impedance ratio of the resistors. In contrast with [4], synchronization circuits are not required between the digitizers and the generators as the algorithm in [6] is used to design the experiment and estimate accurately the signal parameters. In addition, buffer amplifiers to unload the digitizer inputs are not needed as the digitizers are used to sample directly the output voltages of the signal generators. However, techniques to offset the dependence of the injected currents on the impedance of the leads and the current-comparator ratio windings are required.

The paper is organized as follows. The calibration of high-voltage standard capacitors with capacitance and dissipation factor standards and bridges is briefly reviewed in section 2. The construction of dissipation factor standards

is discussed in section 3. The operating principle of the calibration system proposed here is presented in section 4. The measurement procedure is detailed in section 5. The characteristics and the construction of the error-current injection amplifiers are discussed in section 6. The measurement uncertainties are reported in section 7. Experimental results are discussed in section 8. The conclusions are drawn in section 9.

A two-page summary of this paper was published in [7]. An extended version of that paper was accepted for publication in [8]. The paper here addresses further developments performed after the submittal of the paper in [8].

2. THEORY

A high-voltage source, a standard capacitor with known capacitance C_S and dissipation factor tan δ_S, and a capacitance and dissipation factor bridge are required to measure the unknown capacitance C_X and dissipation factor tan δ_X of a test capacitor at power frequencies ω (Fig. 1).

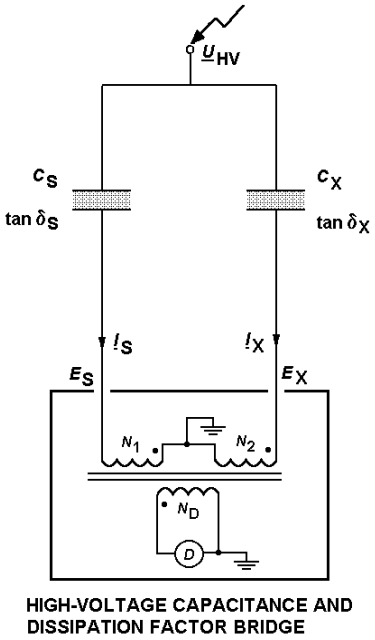

Fig. 1. Measurement system at high voltage.

On the high-voltage side, the standard capacitor and the test capacitor are connected to the high voltage $\underline{U}_{HV}$ (with amplitude $|\underline{U}_{HV}|$ and phase δ_U) and the low-voltage terminals are connected to the inputs E_S and E_X of the bridge (which are nearly at ground potential). The bridge measures the complex ratio of the input currents $\underline{I}_S$ and $\underline{I}_X$. Assuming that lossy capacitors are modeled as a series circuit of reactance $1/\omega C$ and loss resistance R, where the dissipation factor (loss tangent) tan $\delta = D = \omega CR$, the amplitudes of the input currents are

$$|\underline{I}_S| = \frac{\omega C_S |\underline{U}_{HV}|}{\sqrt{1+\tan^2\delta_S}}$$
$$|\underline{I}_X| = \frac{\omega C_X |\underline{U}_{HV}|}{\sqrt{1+\tan^2\delta_X}} \quad (1)$$

and the corresponding phases are

$$\arg \underline{I}_S = \delta_U + \pi/2 - \delta_S$$
$$\arg \underline{I}_X = \delta_U + \pi/2 - \delta_X \quad (2)$$

From these currents, the bridge evaluates the amplitude ratio and the phase displacement

$$\frac{|\underline{I}_X|}{|\underline{I}_S|} = \frac{C_X}{C_S} \cdot \sqrt{\frac{1+\tan^2\delta_S}{1+\tan^2\delta_X}}$$
$$\arg \underline{I}_X - \arg \underline{I}_S = \delta_S - \delta_X \quad (3)$$

Assuming a nondissipative standard capacitor (tan $\delta_S = 0$), the dissipation factor tan δ_X and the capacitance C_X of the test capacitor can be calculated directly from the ratio and the phase displacement of the input currents, that is

$$\tan\delta_X = -\tan(\arg \underline{I}_X - \arg \underline{I}_S)$$
$$C_X = \frac{|\underline{I}_X|}{|\underline{I}_S|} \cdot C_S \cdot \sqrt{1+\tan^2\delta_X} \quad (4)$$

3. DISSIPATION FACTOR STANDARDS

Dissipation factor standards can also be used to calibrate the dissipation factor function of high voltage capacitance bridges. One needs a known standard capacitor C_S with negligible dissipation factor (tan $\delta_S = 0$) and a dissipation factor standard with known capacitance C_X and known dissipation factor tan δ_X.

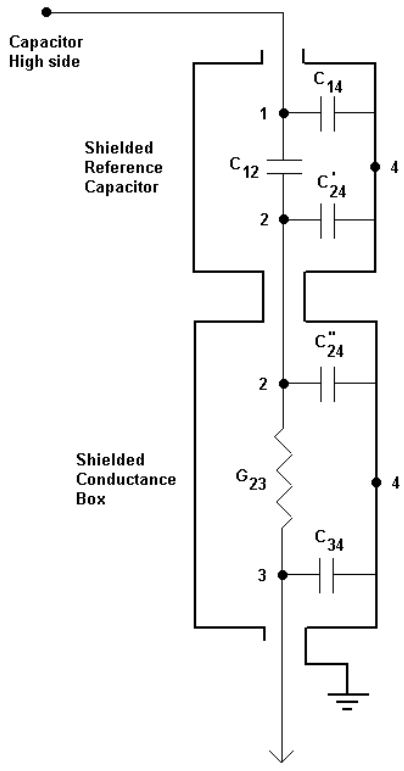

Fig. 2. Dissipation factor standard.

Such standards consist of a series-connected (parallel arrangements can also used but are not studied here) three-terminal standard gas capacitor and a three-terminal conductance, shown schematically in Fig. 2, where C_{12} is the direct capacitance of the shielded reference capacitor, G_{23} is the conductance between the terminals of the shielded conductance box, and C_{14}, C_{34} and C_{24} are stray capacitances to ground. Note that C_{24} comprises the sum of two parallel ground capacitances, C_{24}' and C_{24}", of the component boxes and coupling connector. The design is similar to that described in [3].

It is straightforward to show that the dissipation factor of the network is [3]

$$\tan\delta_X = \omega(C_{12} + C_{24})/G_{23} \tag{5}$$

Also the effective parallel capacitance C_{13} and conductance G_{13} of the network is

$$\begin{aligned} C_{13} &= C_{12}/\left(1+\tan\delta_X^2\right) \\ G_{13} &= \omega C_{12}\tan\delta_X/\left(1+\tan\delta_X^2\right) \end{aligned} \tag{6}$$

The equivalent capacitance C_{13} is the original three-terminal capacitance C_{12} reduced by a factor of $(1+\tan\delta_X^2)^{-1}$. The dissipation factor $\tan\delta_X$, as seen from (5), is directly influenced by the presence of the combined stray junction capacitance to ground C_{24} and therefore a very stable and reproducible value for this capacitance is necessary after reassembling the standard or changing the series conductance box. It is desirable to keep the combined stray junction capacitance C_{24} as small as possible relative to C_{12}.

The dissipation factor standards should have stable values of dissipation factor $\tan\delta_X$ and capacitance C_{13} as defined by (5) and (6), respectively. A highly stable capacitance C_{12} should be used. A gas dielectric, hermetically sealed, three-terminal standard capacitor with nominal value of 1000 pF was chosen. This capacitor has GR874 connectors. The direct capacitance C_{12} of the standard capacitor was determined at 400 Hz, 800 Hz, 1 kHz and 1.6 kHz with an accurate coaxial capacitance bridge [9]. The value at 60 Hz was predicted to be (999.992 ± 0.002) pF using regression techniques [10].

The resistors should be stable with a temperature dependence of less than 10^{-5}/°C, and have negligible time constant at 50-60 Hz (time constant less than 10^{-7} s). The resistance values should be selected to match the measured capacitance values C_{12} and C_{24}, and produce the desired $\tan\delta_X$ from (5). Five conductance boxes were built. Four of them contain hermetically-sealed, H-type Vishay precision resistors with the nominal values: 100 Ω, 500 Ω, 5 kΩ and 50 kΩ. One box contains a 294 kΩ metal-film resistor. Each nickel-plated conductance box has dimensions: 35 x 35 x 75 mm. The box has an N-type input connector and a BNC-type output connector.

The standard capacitor and the conductance box were connected with N-type coaxial connector and adapters to ensure a very stable and reproducible value for the stray capacitance C_{24}. Two adapters were in fact needed: a GR874-N adapter and an N-N adapter. The combined stray ground capacitance value C_{24}, which includes both the internal ground capacitance of the standard capacitor C_{24}' (= 66.4 pF) and that for the conductance box C_{24}" (= 11.7 pF) was determined with a commercial low-frequency impedance analyzer to be (78 ± 4) pF.

Table I lists the standard uncertainties associated with the dissipation factor that can be obtained with this method. As stated in the introduction, this method has some shortcomings: a high-voltage apparatus is required, the number of test points is restricted to the number and values of the standards available, and the dissipation factor uncertainty increases with the actual dissipation factor being measured (this is due to the uncertainty contribution associated with the measurement of the combined stray junction capacitance to ground C_{24}).

TABLE I
DISSIPATION FACTOR[1]

Nominal Dissip.Factor	$u(D_X)$ (k = 1)
$5\cdot10^{-5}$	0.000003
$2\cdot10^{-4}$	0.000003
$2\cdot10^{-3}$	0.000005
$2\cdot10^{-2}$	0.000043
$1\cdot10^{-1}$	0.00025

([1]) C_X/C_S = 1:1.

The operating principle of a new approach designed to overcome those problems is detailed in the next section.

4. OPERATING PRINCIPLE

The new measurement system for the calibration of high-voltage capacitance and dissipation factor bridges is depicted in Fig. 3. The output voltages of two synchronized, programmable signal generators (GEN1 and GEN2) [11] are applied to the inputs E_S and E_X of the bridge under test via two calibrated resistors with impedances $\underline{Z}_1$ and $\underline{Z}_2$ (with ac resistances $|\underline{Z}_1|$ and $|\underline{Z}_2|$, and phase angles arg $\underline{Z}_1$ and arg $\underline{Z}_2$, respectively). Two high-resolution, integrating digital sampling voltmeters in a master-slave configuration [12] (DVM1 – master and DVM2 – slave) are used to measure the voltages $\underline{V}_1$ and $\underline{V}_2$ (with amplitudes $|\underline{V}_1|$ and $|\underline{V}_2|$, and phases arg $\underline{V}_1$ and arg $\underline{V}_2$, respectively) applied to both the resistors and the current-comparator ratio windings (N_1 and N_2). The errors caused by the impedances of N_1 and N_2 (and interconnecting leads) are automatically corrected with amplifier circuits (A_1 and A_2, respectively) that provide the error currents (see section 6 for construction details).

The two DVMs, controlled by the algorithm in [6], can measure the amplitude ratio $|\underline{V}_2|/|\underline{V}_1|$ and the phase displacement arg $\underline{V}_2$ − arg $\underline{V}_1$ of the two output voltage signals with an uncertainty of a few parts in 10^6 and a few microradians, respectively.

The amplitude ratio and the phase displacement of the input currents are therefore

$$\begin{aligned} \frac{|\underline{I}_X|}{|\underline{I}_S|} &= \frac{|\underline{V}_2|}{|\underline{V}_1|}\cdot\frac{|\underline{Z}_1|}{|\underline{Z}_2|} \\ \arg\underline{I}_X - \arg\underline{I}_S &= \arg\underline{V}_2 - \arg\underline{V}_1 + \arg\underline{Z}_1 - \arg\underline{Z}_2 \end{aligned} \tag{7}$$

Well-defined resistors with high stability and low residual reactances are available in metallic film units and resistors of this type are used. Their impedance ratio should preferably be evaluated. However, the resistance ratio at power frequencies can be estimated from the dc resistance ratio R_2/R_1 within a few parts in 10^6. In addition, by symmetrical construction the phase angles of the resistors may be assumed equal within a few microradians. With these simplifying assumptions,

$$\frac{|\underline{I}_X|}{|\underline{I}_S|} = \frac{|\underline{V}_2|}{|\underline{V}_1|} \cdot \frac{R_1}{R_2}$$
$$\arg \underline{I}_X - \arg \underline{I}_S = \arg \underline{V}_2 - \arg \underline{V}_1 \tag{8}$$

Assuming a nondissipative standard capacitor, i.e., $\tan \delta_S = 0$, the reference values of dissipation factor and capacitance ratio for an unknown capacitor are, from (4) and (8),

$$\tan \delta_{X\,ref} = -\tan\left(\arg \underline{V}_2 - \arg \underline{V}_1\right)$$
$$\left(\frac{C_X}{C_S}\right)_{ref} = \frac{|\underline{V}_2|}{|\underline{V}_1|} \cdot \frac{R_1}{R_2} \sqrt{1 + \tan^2 \delta_{X\,ref}} \tag{9}$$

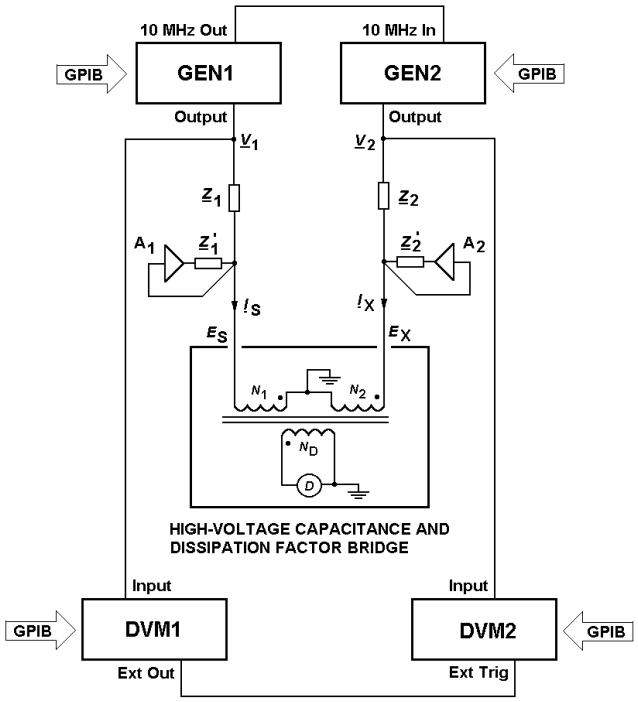

Fig. 3. Calibration system.

5. MEASUREMENT PROCEDURE

DVM1 (master) assumes the role of establishing the timing for the whole sampling process. DVM2 (slave) is configured for external triggering; it samples its input signal only when DVM1 sends (through an output connector of the instrument) a digital signal to the trigger input of DVM2 indicating when a reading is being carried out. Therefore, the digital circuits of the two converters are linked through a fixed delay.

The fundamental frequency f_0 can be known from the number of null-crossings of the signal applied to DVM1. The sampling parameters are evaluated as in [13] (see Table II). A total of n acquisitions of N samples at times $t_i = it_{samp}$, $i = 0, 1, \ldots, N-1$, are taken. The internal level trigger of DVM1 is used to start each k-th acquisition ($k = 0, \ldots, n-1$) delayed by kt_D from a signal null crossing, where t_D approaches $1/nf_0$. The corresponding acquisitions of DVM2 are delayed by kt_D+d from those signal null-crossings, where d is the delay between the two time series due to the external trigger delay and the DVM phase responses. The A/D converter aperture times of both DVMs are selected to prevent trigger-too-fast errors ($t_{aper} = t_{samp} - 0.00003$ s) [13].

TABLE II
SAMPLING PARAMETERS

Parameter	50 Hz	60 Hz
n	12	12
N	1127	1144
t_{samp}	0.001118 s	0.001049 s
t_{aper}	0.001088 s	0.001019 s
f_0	49.998997 Hz	59.998814 Hz
$2\pi f_0 d$	155.10 µrad	186.13 µrad

It is assumed that each acquisition can be fitted with a truncated Fourier series with three harmonics (this is reasonable as low-distortion signal sources are being used to generate the sinusoidal signals). The model assumes that the data set has a zero mean value (any nonzero average value has been subtracted from the data). In matrix notation,

$$\mathbf{y}_{pk} = \mathbf{W}_{pk} \mathbf{x}_p \,, \tag{10}$$

where the subscript p = 1 for DVM1 and p = 2 for DVM2, $\mathbf{y}_{pk}$ is the N-data vector at the k-th acquisition for each DVM, $\mathbf{W}_{1k}$ is the known $N \times 6$ matrix with (i, j)-th element $\cos[2\pi j f_0(t_i+kt_D)]$ for $j = 1, 2, 3$ and $\sin[2\pi(j-3)f_0(t_i+kt_D)]$ for $j = 4, 5, 6$, $\mathbf{W}_{2k}$ is the known $N \times 6$ matrix with (i, j)-th element $\cos[2\pi j f_0(t_i+kt_D+d)]$ for $j = 1, 2, 3$ and $\sin[2\pi(j-3)f_0(t_i+kt_D+d)]$ for $j = 4, 5, 6$, and $\mathbf{x}_p$ is the 6-vector of fitting parameters for each DVM, uncorrected for the systematic effects.

The vector $\mathbf{x}_p$ is estimated from the average of the discrete Fourier transforms over all acquisitions [14][15]

$$\mathbf{x}_p = \frac{2}{nN} \sum_{k=0}^{n-1} \mathbf{W}'_{pk} \mathbf{y}_{pk} \tag{11}$$

where the prime (′) means transpose.

Denoting by $\mathbf{x}_p(j)$ the j-th element of $\mathbf{x}_p$, the fundamental voltage amplitude ratio and phase displacement are

$$\frac{|\underline{V}_2|}{|\underline{V}_1|} = \frac{k_{DC1}}{k_{DC2}} \cdot \frac{\sqrt{\mathbf{x}_2^2(1) + \mathbf{x}_2^2(4)}}{\sqrt{\mathbf{x}_1^2(1) + \mathbf{x}_1^2(4)}}$$
$$\arg \underline{V}_2 - \arg \underline{V}_1 = \tan^{-1}\left[-\frac{\mathbf{x}_2(4)}{\mathbf{x}_2(1)}\right] - \tan^{-1}\left[-\frac{\mathbf{x}_1(4)}{\mathbf{x}_1(1)}\right] \tag{12}$$

where k_{DC1}/k_{DC2} is the ratio of the corrections for the dc voltage mode error of each DVM.

The above equations require knowledge of the delay d and the ratio k_{DC1}/k_{DC2}. In order to evaluate them, an initial voltage measurement is done with GEN1 output signal applied to both DVMs (GEN2 output is now left disconnected). In this case, the reported voltage amplitude ratio and phase displacement should ideally be unity and null degree, respectively. The algorithm measures the uncorrected values (assuming $d = 0$ and $k_{DC1}/k_{DC2} = 1$) and evaluates the delay d and the ratio k_{DC1}/k_{DC2} so that the readings 1.000000 and 0.0000° are reported for the amplitude ratio and phase displacement, respectively. The corrections are very stable [6][12] and are used in the subsequent measurements.

The two DVMs are then connected as described in Fig. 3 to measure the amplitude ratio $|\underline{V}_2|/|\underline{V}_1|$ and the phase displacement arg $\underline{V}_2$ − arg $\underline{V}_1$ of the two output voltage signals. The measured values are then inserted in (9) to obtain the reference values of capacitance ratio and dissipation factor for an unknown capacitor.

The calibration system can simulate any capacitance ratio from 1:1 to 10:1 (other capacitance ratios can be simulated by using resistors of different values) and any dissipation factor from 0 to 1 (or more) at power frequencies. For standardization purposes, the control software allows the user to simulate (a) integer capacitance ratios from 1:1 to 10:1 at a dissipation factor of $1\cdot10^{-6}$ or (b) decadic dissipation factors from $1\cdot10^{-6}$ to 1 at 1:1 capacitance ratio. The corresponding amplitude ratio and phase displacement of the two voltage signals are then set and measured automatically. The fine adjustment of the signal generators however may require user intervention. The reference values of capacitance ratio and dissipation factor are then reported. Several repetitions are made to evaluate the experimental standard deviation of the reference values due to the stability of the generators. The average of the reference values over all those repetitions is finally reported. The whole measuring process takes about two minutes for each test point. The electronic bridge is set to the specific test point and its readings are compared with the simulated reference values reported by the calibration system.

6. CONSTRUCTION OF THE AMPLIFIERS

Battery-operated amplifier circuits are needed to offset the dependence of the injected currents on the impedance of the leads and the current-comparator ratio windings. They inject the error currents. Such amplifiers have been used extensively in current-comparator-based bridges [16][17].

The basic circuit of the amplifier A_1 is shown in Fig. 4 (the circuit of the amplifier A_2 is similar). Assuming a voltage drop $\underline{\xi}_1$ across the current comparator ratio winding N_1 (and interconnecting leads), the voltage drop across the impedance $\underline{Z}_1$ in Fig. 3 is $\underline{V}_1 - \underline{\xi}_1$ and the error current is then $\underline{\xi}_1/\underline{Z}_1$. The amplifier outputs a voltage $2\underline{\xi}_1$ so that the current $\underline{\xi}_1/\underline{Z}_1'$ is injected. This current is nearly equivalent to the error current since $\underline{Z}_1'$ and $\underline{Z}_1$ are equal in magnitude to R_1.

For instance, assuming that $|\underline{V}_1| = 1$ V, $R_1 = 5$ kΩ and that the current comparator ratio winding N_1 has a resistance of about 1 Ω and negligible leakage inductance, the error current is 0.04 μA or two parts in 10^4 of the test current (0.2 mA). Therefore, precision resistors with 0.1% tolerance are required in the amplifier to provide the error current within a few parts in 10^7. The precision requirement is less stringent for $R_1 = 50$ kΩ, where the error current is 0.4 nA or two parts in 10^5 of the test current (0.02 mA). The lower the resistor values are the more precise they should be.

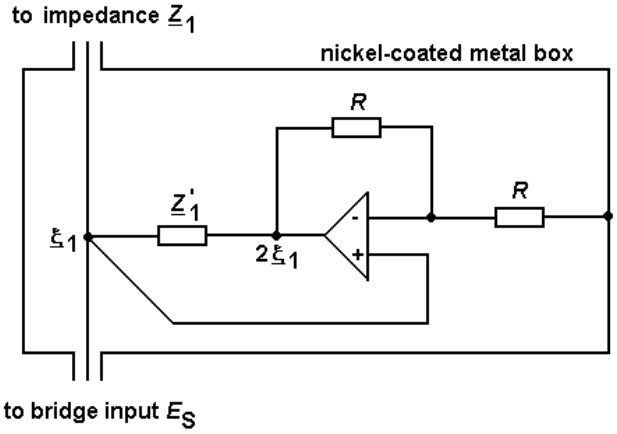

Fig. 4. Amplifier circuit A_1.

The resistor and amplifier boxes have a coaxial design (Fig. 5). Both are nickel-coated to reduce the contact resistances. The output voltages of the signal generators are sampled by the digital voltmeters through the connectors on top of the resistor boxes. This is done to avoid the voltage drops in the output leads of the signal generators.

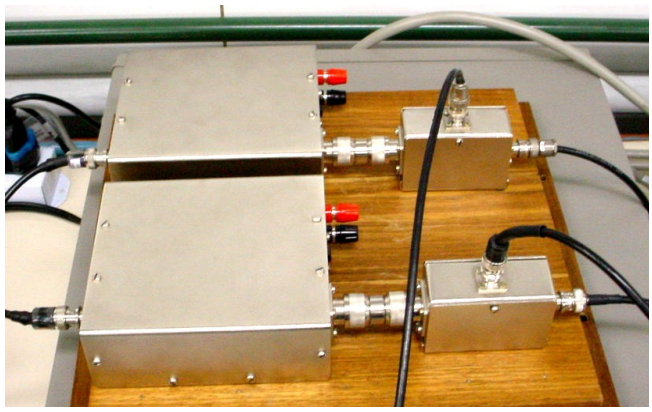

Fig. 5 Amplifier boxes (left) and resistor boxes (right).

We have recently verified that sometimes the bridge under calibration became damaged immediately after conducting the test. An investigation has been made to solve the problem. It was found that the cause was an unbalance in the outputs of the $+V_{CC}$ and the $-V_{CC}$ voltage regulators that feed the operational amplifier. The solution was to insert a parallel RC circuit between those outputs as illustrated in Fig. 6. The scheme also shows the means used to switch off the circuit and to allow the batteries to be loaded. We chose the operational amplifier OP07 for its accuracy and stability combined with its freedom from external offset nulling. The stability of offsets and gain with time and variations in temperature of such amplifier is excellent.

7. MEASUREMENT UNCERTAINTY

Commercial electronic bridges based on [1][2] have been calibrated at $|\underline{I}_S|$ = 0.2 mA (and $|\underline{I}_S|$ = 0.02 mA) with the system described above using $R_1 = R_2 = 5$ kΩ (and $R_1 = R_2 =$ 50 kΩ). More recently, such bridges have also been calibrated with $R_1 = 50$ kΩ and $R_2 = 5$ kΩ for capacitance ratios from 10:1 to 100:1.

The standard uncertainties associated with the simulated reference values of capacitance ratio and dissipation factor at $|\underline{I}_S|$ = 0.2 mA are listed in Table III and Table IV, respectively. In addition, the standard uncertainties at $|\underline{I}_S|$ = 0.02 mA are listed in Table V and Table VI. The standard uncertainties for capacitance ratios from 10:1 to 100:1 are listed in Table VII. They were evaluated from (9) by applying the GUM rules [18]. The figures include the contribution associated with the stability of the generators.

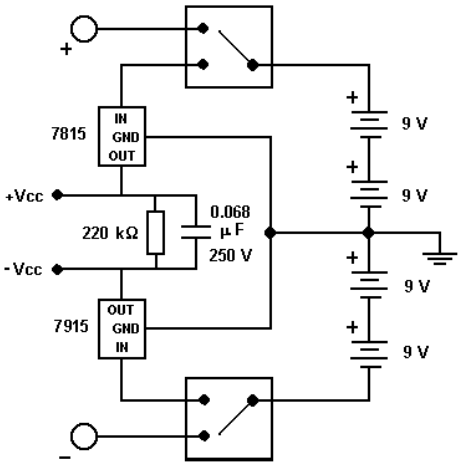

Fig. 6. Amplifier circuit A_1.

TABLE III
CAPACITANCE RATIO[1]

Nominal Cap. Ratio	$u((C_X/C_S)_{ref})$ (k = 1)
1:1	0,000009
2:1	0,000014
3:1	0,000036
4:1	0,000033
5:1	0,000050
6:1	0,00011
7:1	0,00012
8:1	0,00012
9:1	0,00020
10:1	0,00021

([1]) $D_X = 1 \cdot 10^{-6}$ and $|\underline{I}_S|$ = 0.2 mA.

TABLE IV
DISSIPATION FACTOR[1]

Nominal Dissip.Factor	$u(D_{Xref})$ (k = 1)
$1 \cdot 10^{-6}$	0,000006
$1 \cdot 10^{-5}$	0,000006
$1 \cdot 10^{-4}$	0,000006
$1 \cdot 10^{-3}$	0,000008
$1 \cdot 10^{-2}$	0,000006
$1 \cdot 10^{-1}$	0,000012

([1]) C_X/C_S = 1:1 and $|\underline{I}_S|$ = 0.2 mA.

TABLE V
CAPACITANCE RATIO[1]

Nominal Cap. Ratio	$u((C_X/C_S)_{ref})$ (k = 1)
1:1	0,000017
2:1	0,000029
3:1	0,000058
4:1	0,000055
5:1	0,00012
6:1	0,00014
7:1	0,00015
8:1	0,00011
9:1	0,00012
10:1	0,00023

([1]) $D_X = 1 \cdot 10^{-6}$ and $|\underline{I}_S|$ = 0.02 mA.

TABLE VI
DISSIPATION FACTOR[1]

Nominal Dissip.Factor	$u(D_{Xref})$ (k = 1)
$1 \cdot 10^{-6}$	0,000005
$1 \cdot 10^{-5}$	0,000005
$1 \cdot 10^{-4}$	0,000005
$1 \cdot 10^{-3}$	0,000005
$1 \cdot 10^{-2}$	0,000004
$1 \cdot 10^{-1}$	0,000006

([1]) C_X/C_S = 1:1 and $|\underline{I}_S|$ = 0.02 mA.

TABLE VII
CAPACITANCE RATIO[1]

Nominal Cap. Ratio	$u((C_X/C_S)_{ref})$ (k = 1)
10:1	0,000084
20:1	0,00015
30:1	0,00026
40:1	0,00054
50:1	0,00045
60:1	0,00085
70:1	0,00054
80:1	0,00097
90:1	0,0015
100:1	0,0021

([1]) $D_X = 1 \cdot 10^{-6}$ and $|\underline{I}_S|$ = 0.02 mA.

8. EXPERIMENTAL RESULTS

Examples of simulated reference values of capacitance ratio and dissipation factor at $|\underline{I}_S|$ = 0.2 mA and the corresponding average readings of the bridge based on [1] are listed in Table VIII and Table IX, respectively. Tables X and XI list the figures obtained for the bridge based on [2] which has a resolution of $1 \cdot 10^{-6}$ for both capacitance ratio and dissipation factor measurements. Table XII shows the results obtained for capacitance ratios from 10:1 to 100:1 for the bridge based on [2]. The tables also list the expanded uncertainties (k = 2) associated with the reference values.

The differences between the reference values and the average readings are in general well within those expanded uncertainties. The differences for high values of dissipation factor actually exceed the expanded uncertainties, but the manufacturers do recognize this by suitably decreasing the accuracy claims for such values in their product specifications.

TABLE VIII
CAPACITANCE RATIO[1]

$(C_X/C_S)_{ref}$	$U((C_X/C_S)_{ref})$ ($k = 2$)	Reading of bridge [1]
1.000257	0.000084	1.0003
1.999725	0.000086	1.9997
3.00145	0.00016	3.0014
4.00039	0.00013	4.0004
5.00078	0.00019	5.0008
6.00040	0.00017	6.0003
6.99893	0.00019	6.9989
8.00187	0.00030	8.0019
9.00287	0.00041	9.0029
9.99803	0.00031	9.9980

([1]) $D_X = 1 \cdot 10^{-6}$ and $|\underline{I}_S| = 0.2$ mA.

TABLE IX
DISSIPATION FACTOR[1]

D_{Xref}	$U((D_{Xref})$ ($k = 2$)	Reading of bridge [1]
0.000004	0.000014	0.00001
0.000022	0.000014	0.00004
0.000105	0.000016	0.00012
0.000998	0.000016	0.00100
0.010002	0.000021	0.00995
0.099992	0.000029	0.09943
1.00008	0.00085	0.99779

([1]) $C_X/C_S = 1{:}1$ and $|\underline{I}_S| = 0.2$ mA.

TABLE X
CAPACITANCE RATIO[1]

$(C_X/C_S)_{ref}$	$U((C_X/C_S)_{ref})$ ($k = 2$)	Reading of bridge [2]
1.000277	0.000025	1.000274
1.999839	0.000032	1.999854
2.99979	0.00010	2.999801
4.000175	0.000070	4.000179
5.00033	0.00013	5.000291
6.00002	0.00029	5.999980
6.99892	0.00026	6.998971
7.99731	0.00038	7.997351
8.99325	0.00041	8.993379
9.99735	0.00048	9.997315

([1]) $D_X = 1 \cdot 10^{-6}$ and $|\underline{I}_S| = 0.2$ mA.

TABLE XI
DISSIPATION FACTOR[1]

D_{Xref}	$U((D_{Xref})$ ($k = 2$)	Reading of bridge [2]
-0.000009	0.000012	-0.000009
0.000010	0.000012	0.000012
0.000098	0.000012	0.000096
0.000987	0.000016	0.000984
0.009994	0.000012	0.009958
0.100020	0.000024	0.099679

([1]) $C_X/C_S = 1{:}1$ and $|\underline{I}_S| = 0.2$ mA.

TABLE XII
CAPACITANCE RATIO[1]

$(C_X/C_S)_{ref}$	$U((C_X/C_S)_{ref})$ ($k = 2$)	Reading of bridge [2]
10,00130	0,00021	10,00135
20,00303	0,00032	20,00314
29,99826	0,00055	29,99858
40,0026	0,0015	40,00319
49,99751	0,00090	49,99814
60,0201	0,0026	60,02179
69,9993	0,0013	70,00066
79,9896	0,0027	79,99240
89,9988	0,0054	90,00114
100,0554	0,0042	100,0581

([1]) $D_X = 1 \cdot 10^{-6}$ and $|\underline{I}_S| = 0.2$ mA.

9. CONCLUSION

A new approach for calibrating automated high-voltage current-comparator-based capacitance and dissipation factor bridges has been presented. Input currents from tens of μA to a few mA at power frequencies are synthesized as required for the calibration of such bridges. The ratio and phase displacement of the input currents are estimated from the digitized data using an optimized algorithm for nonsynchronous sampling. The estimates are used to calculate the reference values of capacitance ratio and dissipation factor. The calibration system uses commercially available equipment. It is possible to simulate capacitance ratios from 1:1 to 100:1 with relative standard uncertainties of less than $2.5 \cdot 10^{-5}$ and dissipation factors from 0 to 0.1 with standard uncertainties of less than $1 \cdot 10^{-5}$. The method has been applied to the calibration of commercial electronic bridges. It is a refinement of an approach described earlier. It leads to larger uncertainties, but is slightly easier to implement, since the digitizers need not be synchronized to the signal generators.

AKNOWLEDGMENTS

Prof. Endre Tóth (in memoriam) constructed at Inmetro the dissipation factor standards discussed in section 3 that had been used in an old calibration system. Renata Teixeira de Barros Vasconcellos helped me with the operation of the old system after he passed away.

Renata also participated in an early stage of this new development and helped me with the initial tests. I thank her for that. I thank also Flavio Senna Acon and Dimas Barbosa Teixeira for building the amplifiers. They did a great job. I am also very grateful to Alexandre Etchebehere for suggesting and implementing the solution (illustrated in Fig. 6) to the amplifier problem reported. Ronaldo Miloski Pessurno was also very instrumental in providing resources for this work. I thank also Flavia Noêmia Cerqueira Leite Geraldo for helping me with recent calibration tests for customers. Finally, I wish to thank Luiz Macoto Ogino for providing the resources for this work.

REFERENCES

[1] P. Osvath and S. Widmer, "High-voltage high-precision self-balancing capacitance and dissipation factor bridge for industrial measurements", *4th Int. Symp. High Voltage Engineering Conf. Dig.*, Athens, Greece, Sep. 5-9, 1983, pp. 64.01-03.

[2] E. So, "A microprocessor-controlled high-voltage current-comparator-based capacitance bridge", *IEEE Trans. Pow. Deliv.*, 5, no. 2, pp. 533-537, Apr. 1990.

[3] R. D. Simmon, G. J. FitzPatrick and O. Petersons, "Calibration of dissipation factor standards", *IEEE Trans. Instrum. Meas.*, 48, no. 2, pp. 450-452, Apr. 1999.

[4] G. Ramm and H. Moser, "Calibration of electronic capacitance and dissipation factor bridges", *IEEE Trans. Instrum. Meas.*, 52, n. 2, pp. 396-399, Apr. 2003.

[5] G. Ramm, H. Moser and A. Braun, "A new scheme for generating and measuring active, reactive, and apparent power at power frequencies with uncertainties of 2.5 x 10^{-6}", *IEEE Trans. Instrum. Meas.*, 48, no. 2, pp. 422-426, Apr. 1999.

[6] G. A. Kyriazis and M. L. R. Campos, "An algorithm for accurately estimating the harmonic magnitudes and phase shifts of periodic signals with asynchronous sampling", *IEEE Trans. Instrum. Meas.*, 54, no. 2, pp. 496-499, Apr. 2005.

[7] G. A. Kyriazis, "Calibration of high-voltage current-comparator-based bridges using nonsynchronous digital sampling, *CPEM Digest*, Broomfield, USA, Jun. 2008, pp. 198-199.

[8] G. A. Kyriazis, "Calibration of high-voltage current-comparator-based bridges using nonsynchronous digital sampling, *IEEE Trans. Instrum. Meas.*, 58, no. 2, Apr. 2009, in publication.

[9] G. A. Kyriazis, R. T. B. Vasconcellos, L. M. Ogino *et al.*, "Design and construction of a two terminal-pair coaxial capacitance bridge", in *Proc. of the VI SEMETRO*, pp. 57-62, Rio de Janeiro, Sep. 21-23, 2005.

[10] G. M. Rocha and G. A. Kyriazis, "A software for the evaluation of the stability of measuring standards using Bayesian statistics", in *Proc. 13th IMEKO International Symposium on Measurements for Research and Industry Applications*, v. 1, pp. 386-391, Athens, Sep.29-Oct.1, 2004.

[11] Agilent 33250A, *80 MHz Function/Arbitrary Waveform Generator – User's Guide*, Ed. 2, Aug. 2002.

[12] U. Pogliano, "Use of integrative analog-to-digital converters for high-precision measurement of electrical power", *IEEE Trans. Instrum. Meas.*, 50, no. 5, pp. 1315-1318, Oct. 2001.

[13] R. L. Swerlein, "A 10 ppm accurate digital ac measurement algorithm", *Proc. NCSL Workshop and Symposium*, Albuquerque, Aug. 1991, pp. 17-36. Available: http://www.agilent.com.

[14] G. A. Kyriazis and M. L. R. Campos, "Bayesian inference of linear sine-fitting parameters from integrating digital voltmeter data", *Meas. Sci. Tech.*, 15, pp. 337-346, Feb. 2004. Erratum: pp. 1047.

[15] G. A. Kyriazis, "An orthogonal design of experiments for accurately estimating harmonics of low frequency periodic signals", *IEEE Latin America Transactions*, 6, no. 1, pp. 1-8, Jan. 2008. In Portuguese.

[16] W. J. M. Moore and K. Ayukawa, "A current comparator bridge for power measurement", *IEEE Trans. Instrum. Meas.*, 25, pp. 550-553, Dec. 1976.

[17] G. A. Kyriazis, N. M. Oldham and M. Werneck, "A current-comparator-based bridge for calibrating power and energy standards at 50/60 Hz", *CPEM Digest*, Ottawa, Canada, Jun. 2002, pp. 256-257.

[18] BIPM, IEC, IFCC, ISO, IUPAC, IUPAP and OIML 1995 *Guide to the expression of uncertainty in measurement* (Geneva, Switzerland: International Organization for Standardization).